METHODS
Mars Subsurface Ice Model (MSIM)

Norbert Schörghofer (norbert@psi.edu)
Honolulu, Hawaii

2001–2022
Last updated April 18, 2022

Contents

Preface

Companion to `https://github.com/nschorgh/MSIM/`

Cite source code or the description of methods as:

N. Schörghofer. Mars Subsurface Ice Model (MSIM) Program Collection, 2022. GitHub. https://github.com/nschorgh/MSIM/

Technical Notes:
Most of the code was developed with a `gfortran` compiler on Intel processors. Many components were also run on various Linux clusters, sometimes using other compilers. The non-portable `real(8)` and `real*8` are meant to correspond to an 8-byte floating point number.

Part 1

1D Thermal Model for Mars

1-Dimensional Numerical Model of Thermal Conduction and Surface Energy Balance

The heat flow in the shallow subsurface is described by the heat equation:

$$\rho c \frac{\partial T}{\partial t} = \frac{\partial}{\partial z}\left(k \frac{\partial T}{\partial z}\right) \tag{1.1}$$

where T is temperature, t time, z depth, ρc the volumetric heat capacity, and k thermal conductivity.

The (negative of the) heat flux is $F = k\dfrac{\partial T}{\partial z}$.

Boundary conditions are specified below.

1.1   Semi-Implicit Scheme on Irregular Grid

Authors & History: originally implemented by Samar Khatiwala in 2001 (including upper radiation boundary condition for semi-implicit scheme); extended to variable thermal properties and irregular grid by Norbert Schörghofer 2002–2003; added predictor-corrector step in 2019

A flux-conservative discretization on an irregularly-spaced grid is given by

$$\frac{\partial}{\partial z} F_j = \frac{F_{j+\frac{1}{2}} - F_{j-\frac{1}{2}}}{(z_{j+1} - z_{j-1})/2} = 2 \frac{k_{j+\frac{1}{2}} \frac{T_{j+1} - T_j}{z_{j+1} - z_j} - k_{j-\frac{1}{2}} \frac{T_j - T_{j-1}}{z_j - z_{j-1}}}{z_{j+1} - z_{j-1}}$$

Subscript j refers to position z_j. The spatial discretization of the heat equation (1.1) then becomes

$$
\begin{aligned}
(\rho c)_j \frac{\partial T_j}{\partial t} &= \frac{2 k_{j+\frac{1}{2}}}{(z_{j+1} - z_j)(z_{j+1} - z_{j-1})} T_{j+1} - \frac{2}{z_{j+1} - z_{j-1}}\left(\frac{k_{j+\frac{1}{2}}}{z_{j+1} - z_j} + \frac{k_{j-\frac{1}{2}}}{z_j - z_{j-1}}\right) T_j + \\
&\quad + \frac{2 k_{j-\frac{1}{2}}}{(z_j - z_{j-1})(z_{j+1} - z_{j-1})} T_{j-1}
\end{aligned}
$$

$$\text{introduce} \quad \alpha_j = \frac{\Delta t}{(\rho c)_j} \frac{k_{j+\frac{1}{2}}}{(z_{j+1} - z_j)(z_{j+1} - z_{j-1})} \quad \text{and} \quad \gamma_j = \frac{\Delta t}{(\rho c)_j} \frac{k_{j-\frac{1}{2}}}{(z_j - z_{j-1})(z_{j+1} - z_{j-1})} \tag{1.2}$$

$$\frac{\partial T_j}{\partial t} = 2\alpha_j T_{j+1} - 2(\alpha_j + \gamma_j)T_j + 2\gamma_j T_{j-1}$$

A semi-implicit time discretization of (1.1) is of the form (Crank and Nicolson, 1947; Press et al., 1992)

$$(\rho c)_j \frac{T_j^{n+1} - T_j^n}{\Delta t} = \frac{1}{2}\left(\frac{\partial}{\partial z}F_j^{n+1} + \frac{\partial}{\partial z}F_j^n\right)$$

where superscript n refers to the time step. Hence,

$$T_j^{n+1} - T_j^n = \alpha_j T_{j+1}^{n+1} - (\alpha_j + \gamma_j)T_j^{n+1} + \gamma_j T_{j-1}^{n+1} + \alpha_j T_{j+1}^n - (\alpha_j + \gamma_j)T_j^n + \gamma_j T_{j-1}^n$$

which leads to the system of equations

$$\boxed{-\alpha_j T_{j+1}^{n+1} + (1 + \alpha_j + \gamma_j)T_j^{n+1} - \gamma_j T_{j-1}^{n+1} = \alpha_j T_{j+1}^n + (1 - \alpha_j - \gamma_j)T_j^n + \gamma_j T_{j-1}^n} \quad 1 < j < N$$

$$(1.3)$$

This tridiagonal linear system can be solved in $O(N)$ steps.

Whereas the temperature T_j is defined on grid point z_j, the conductivity k is defined in between points. In the equations above, $(\rho c)_j$ is defined on z_j, but in the program implementations, $2(\rho c)_j = (\rho c)_{j+\frac{1}{2}} + (\rho c)_{j-\frac{1}{2}}$. In this way, the thermal properties k and ρc are defined on the same points. And they do not need to be defined at an interface of two layers with different thermal properties when that interface coincides with a grid point. Since array indices must be integers, we choose $\texttt{k[j]} = k_{j-\frac{1}{2}}$, and the same for ρc.

Although the derivation was made with time-constant thermal parameters k and ρc, it remains valid if these parameters change slowly with time.

1.1.1 Upper boundary condition: Stefan-Boltzmann radiation law

The surface energy balance is given by

$$Q + k\left.\frac{\partial T}{\partial z}\right|_{z=0} = \epsilon\sigma T^4\big|_{z=0} \tag{1.4}$$

Q is the incoming solar flux including any atmospheric contribution. On the right-hand side, ϵ is the (infrared) emissivity of the surface and σ is the Stefan-Boltzmann constant. To apply an implicit method, the nonlinear boundary condition needs to be linearized.

Introduce the auxiliary quantity T_0, such that surface temperature $T_s = (T_0 + T_1)/2$

$$\left.\frac{\partial T}{\partial z}\right|_{z=0} = \frac{T_1 - T_0}{\Delta z} \quad \text{and} \quad T^4\big|_{z=0} = \left(\frac{T_0 + T_1}{2}\right)^4 \quad \text{with} \quad \Delta z = 2z_1$$

$T = T_r + T'$ T_r is a reference temperature around which we linearize

$$Q + k_{1/2}\frac{T_1 - T_0}{\Delta z} = \epsilon\sigma\left(\frac{2T_r + T_0' + T_1'}{2}\right)^4$$

$$\approx \epsilon\sigma T_r^4 + 2\epsilon\sigma T_r^3(T_0' + T_1') = -3\epsilon\sigma T_r^4 + 2\epsilon\sigma T_r^3(T_0 + T_1)$$

$T_0\left(\frac{k_{1/2}}{\Delta z} + B(T_r)\right) = Q + 3\epsilon\sigma T_r^4 + T_1\left(\frac{k_{1/2}}{\Delta z} - B(T_r)\right)$ where $B(T_r) = 2\epsilon\sigma T_r^3$

Introduce $a = (Q + 3\epsilon\sigma T_r^4)/\left(\frac{k}{\Delta z} + B\right)$ and $b = \left(\frac{k_{1/2}}{\Delta z} - B\right)/\left(\frac{k_{1/2}}{\Delta z} + B\right)$.

The relation for $j = 1$ is then

$$-\alpha_1 T_2^{n+1} + (1 + \alpha_1 + \gamma_1 - \gamma_1 b^{n+1}) T_1^{n+1} = \alpha_1 T_2^n + (1 - \alpha_1 - \gamma_1 + \gamma_1 b^n) T_1^n + \gamma_1 (a^n + a^{n+1}) \quad (1.5)$$

Define $\beta = \frac{\Delta t}{(\rho c)_1} \frac{1}{2 \Delta z^2}$, then $\alpha_1 = \beta k_{3/2}$ and $\gamma_1 = \beta k_{1/2}$. The surface temperature is computed as

$$T_s = \frac{1}{2}(T_0 + T_1) = \frac{1}{2}(a + bT_1 + T_1)$$

Choose $T_r^n = T_s^n$. The semi-implicit solver with this boundary condition is implemented in `conductionQ.f90`.

The uppermost layer is a half-layer, and the first few grid points must be chosen as $z_0 = 0$ and $z_2 = 3z_1$ (in other words $z_1 = \Delta z/2$, $z_2 = z_1 + \Delta z$). The coefficients for the nonlinear upper boundary condition are designed for that. Subroutine `setgrid` can be used to generate a suitable grid.

Modified treatment of the upper boundary helpful in some situations: The linearization of the Stefan-Boltzmann law, σT^4, works well as long as the surface temperature changes slowly. The above approximation works very well for most situations, such as Mars orbit and a horizontal surface. A temporary instability, where the surface temperature overshoots significantly, was encountered in two situations: i) A sloped, shadowed surface emerges into sunlight. In this case the energy input changes abruptly. ii) For asteroid orbits with high eccentricity and very small perihelion distances, when the pole emerges from winter into sunlight near perihelion. This transition is continuous, but the change in input energy is nevertheless dramatic.

Above, the thermal emission is linearized around the reference temperature $T_r^n = T_s^n$. If T_s^{n+1} is far from T_s^n, a significant error was incurred in the evaluation of the emitted energy. This can be addressed by repeating the calculation with a new reference temperature T_r somewhere in between T_s^n and T_s^{n+1}. An empirical choice is the geometric mean between the previous reference temperature and the new surface temperature. This method is essentially a predictor-corrector step, iteratively applied until T_r is within 20% of $T_s^{(n+1)}$.

Another approach is "artificial flux smoothing" where the time step is subdivided into many substeps, using linear interpolation of the incoming flux from Q^n to Q^{n+1}. It turns a discontinuous change in Q into a continuous change. However, this approach does not identify a nascent instability or answer how many substeps are required to cure it.

1.1.2   Upper boundary condition: prescribed T

The general formulas (1.2,1.3) with $T_0 = T_s$ and $z_0 = 0$ yield

$$\alpha_1 = \frac{\Delta t}{(\rho c)_1} \frac{k_{3/2}}{(z_2 - z_1) z_2} \quad \text{and} \quad \gamma_1 = \frac{\Delta t}{(\rho c)_1} \frac{k_{1/2}}{z_1 z_2}$$

The relation for $j = 1$ becomes

$$-\alpha_1 T_2^{n+1} + (1 + \alpha_1 + \gamma_1) T_1^{n+1} = \alpha_1 T_2^n + (1 - \alpha_1 - \gamma_1) T_1^n + \gamma_1 (T_s^n + T_s^{n+1}) \quad (1.6)$$

which is implemented in `conductionT.f90`. This is a standard Crank-Nicolson solver for an irregular spaced grid.

1.1.3 Lower boundary condition

(assume $z_{N+1} - z_N = z_N - z_{N-1} =: \Delta z$)

No heat flux: $F_{N+\frac{1}{2}} = 0 \quad \Rightarrow \quad k_{N+\frac{1}{2}}(T_{N+1} - T_N) = 0 \quad \Rightarrow \quad T_{N+1} = T_N$

$$(1 + \gamma_N)T_N^{n+1} - \gamma_N T_{N-1}^{n+1} = (1 - \gamma_N)T_N^n + \gamma_N T_{N-1}^n$$

$$\gamma_N = \frac{\Delta t}{(\rho c)_N} \frac{k_{N-\frac{1}{2}}}{2(z_N - z_{N-1})^2}$$

With geothermal heating: $F_{N+\frac{1}{2}} = F_{\text{geothermal}} \quad \Rightarrow \quad k_{N+\frac{1}{2}}(T_{N+1} - T_N) = \Delta z F_{\text{geothermal}}$

$$(1 + \gamma_N)T_N^{n+1} - \gamma_N T_{N-1}^{n+1} = (1 - \gamma_N)T_N^n + \gamma_N T_{N-1}^n + \frac{\Delta t}{(\rho c)_N} \frac{F_{\text{geothermal}}}{\Delta z} \tag{1.7}$$

1.1.4 Validations

The following tests were performed for these solvers:

a) For a sinusoidally varying surface temperature, the solution to the heat equation is known analytically:

$$T = T_m + T_a e^{-z/\delta} \sin\left(\frac{z}{\delta} - \frac{2\pi t}{P}\right) \tag{1.8}$$

where

$$\delta = \frac{\Gamma}{\rho c}\sqrt{\frac{P}{\pi}} \tag{1.9}$$

is the thermal skin depth, Γ the thermal inertia, and P the period. This expression can be used to validate `conductionT` for uniform thermal properties (Figure 1.1). The heat flux is given by

$$F = -k\frac{\partial T}{\partial z} = -\sqrt{2}\, k \frac{T_a}{\delta} e^{-z/\delta} \cos\left(\frac{z}{\delta} - \frac{2\pi t}{P} + \frac{\pi}{4}\right)$$

b) Convergence of some solutions with Δt and Δz has been verified.

c) For periodic solutions (of `conductionT` and `conductionQ`) the heat flux $F = -k\partial T/\partial z$, time-averaged over one period, must be the same at all depths and equal to the heat flux imposed at the bottom boundary, even for spatially-varying thermal properties, as long as the heat capacity does not vary with time; consider the time average of eq. (1.1). Figure 1.2 shows one example.

d) A short-term solution for the heat equation with Stefan-Boltzmann radiation surface boundary condition was derived by Handelsman and Olmstead (1972). Their non-dimensional equations are $T_t = T_{zz}$, $T_z(0,t) = T^n(0,t) - f(t)$, $T(z,0) = 0$, $\lim_{z\to\infty} T(z,t) = 0$. In our case $n = 4$ and $f(t) = T_e^4$, where T_e is an ambient temperature. In this case, their solution is $T(0,t) = \frac{2}{\sqrt{\pi}}T_e^4\sqrt{t}$, for small t. After re-dimensionalizing, the surface temperature is found to change as

$$T(0,t) = T_0 + \frac{2}{\sqrt{\pi}}\frac{\epsilon\sigma}{\Gamma}\left(T_e^4 - T_0^4\right)\sqrt{t} \qquad \text{for small } t \geq 0 \tag{1.10}$$
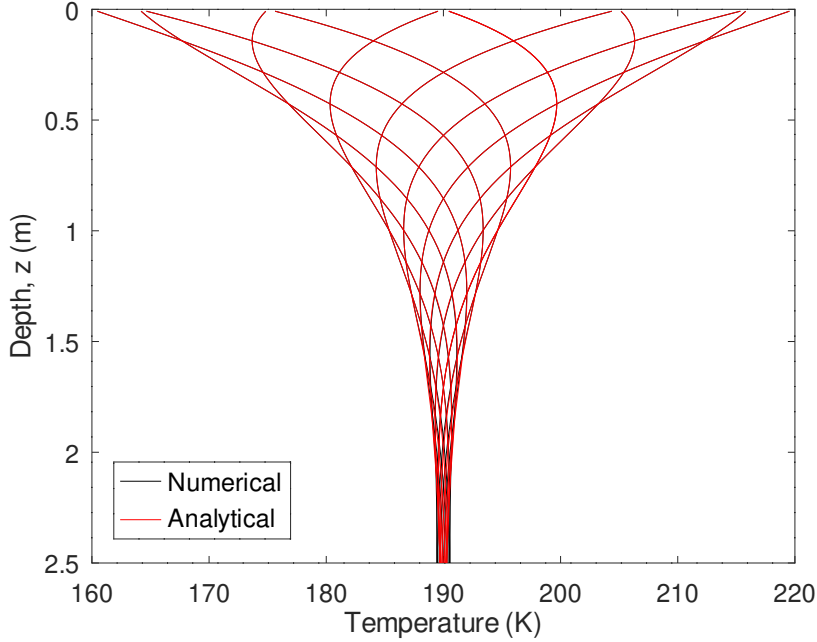
6

Figure 1.1: Comparison of numerical with analytical solution for Crank-Nicolson solver with periodic surface boundary condition. The deviations at the bottom are justified because the analytical solution (1.8) is for an infinitely deep domain. Non-equidistant grid points were used in this example.

where $T_0 = T(0,0)$ is the initial surface temperature. Figure 1.3 shows that the numerical solver reproduces the expected behavior for this discontinuous change in incoming flux.

e) When applied to Mars, modeled surface temperatures have been compared to TES (Thermal Emission Spectrometer) surface temperatures.

1.2 Other Model Components

1.2.1 Seasonal frost cover

The surface energy balance with the latent heat of CO_2 sublimation added is

$$Q + k \left.\frac{\partial T}{\partial z}\right|_{z=0} = \left.\epsilon\sigma T^4\right|_{z=0} + L\frac{dm_{CO_2}}{dt} \quad \text{with} \quad m_{CO_2} \geq 0 \qquad (1.11)$$

where L is the specific latent heat and m_{CO_2} is the areal density of CO_2 ice. Call `conductionQ` if the surface temperature T_s is above the CO_2 frost point temperature or if $m_{CO_2} = 0$. Call `conductionT` if T_s is below the CO_2 frost point or if $m_{CO_2} > 0$. In the latter case, calculate the energy difference and update m_{CO_2}. Adjust the surface albedo and infrared emissivity. Repeat this at every time step. `mars_thermal1d.f` is an implementation of the 1D thermal model for Mars.
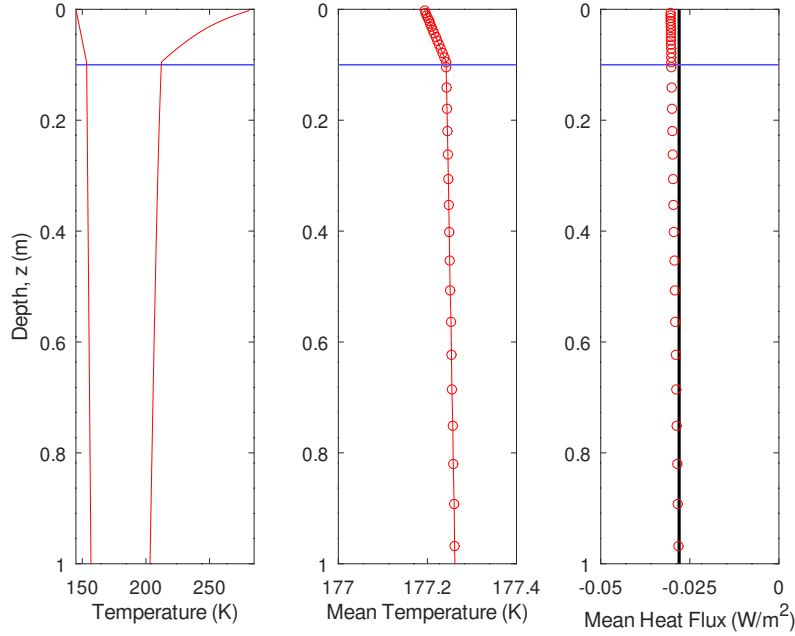
7

Figure 1.2: Validation of the conservation of the heat flux (flux-conservative discretization). The ice table at 10 cm depth causes dramatic changes in thermal properties. Left panel: Minimum and maximum subsurface temperatures over one Mars year. Middle panel: Temperatures averaged over one Mars year, which change linearly as the thermal conductivity is constant within each of the two layers. Right panel: Heat flux averaged over one Mars year, which is preserved across changes in thermal properties and equals to the heat flux imposed at the bottom boundary of 0.028 W/m^2.

The Mars thermal model was used in Schorghofer and Aharonson (2005) and many subsequent papers, including Schorghofer (2008).

1.2.2 Thermal properties of the ground

See Winter and Saari (1969) for heat capacity of silicates as a function of temperature. Notably, many silicates have about the same specific heat capacity. See Handbook of Chemistry and Physics (Lide, 2003) for the temperature dependence of ice. At around 200 Kelvin: $c_{ice} \approx 1540$ J/(kg K), $\rho_{ice} \approx 927$ kg/m^3, $k_{ice} \approx 3.2$ W/(m K), which results in a thermal inertia of 2137 J m^{-2}K^{-1}s$^{-1/2}$. The thermal conductivity of granular media varies by four orders of magnitudes on planetary surfaces, primarily due to the dependence on grain size.

Influence of ice on thermal properties: Ice can greatly change the thermal properties of porous ground. The following is one possible parametrization. In retrospective, it agrees well with the laboratory measurements by Siegler et al. (2012) for vapor-deposited ice.

$$\begin{aligned} \rho c &= (1-\epsilon)\rho_{regolith}c_{regolith} + \epsilon f \rho_{ice}c_{ice} \\ k &= (1-\epsilon)k_{regolith} + \epsilon f k_{ice} + (1-f)\epsilon k_{air} \end{aligned}$$
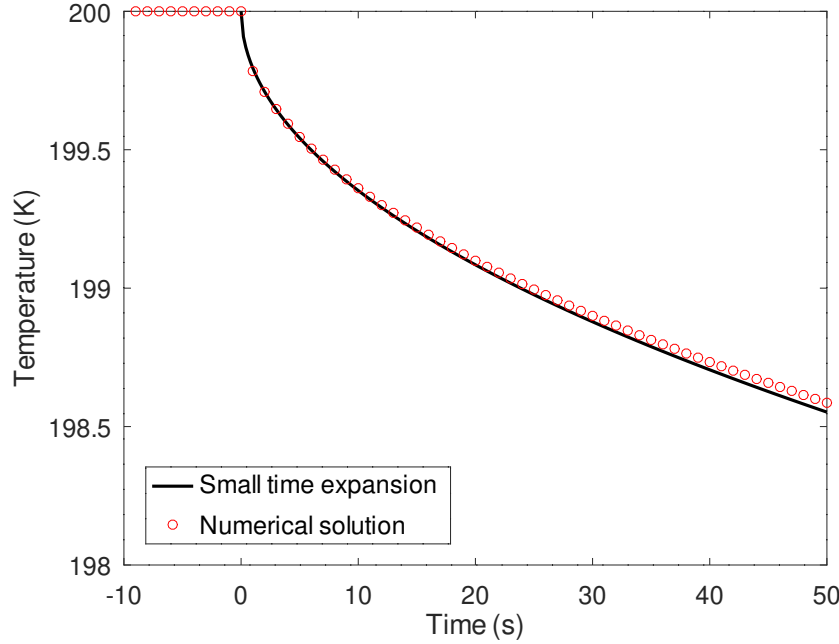
Figure 1.3: Response of numerical solution to a sudden change in incoming flux compared to the analytically obtained expansion for small times, eq. (1.10).

where ρ is density, c heat capacity, k thermal conductivity, ϵ porosity (void space / total volume), and f the ice filling fraction ($f = \rho_f/\rho_{\text{ice}}$, ρ_f =density of free ice).

In the program, k and ρc are defined halfway between grid points, whereas ρ_f and T are defined on grid points.

The thermal inertia of ice-cemented soil is not drastically different from pure ice, which lends some justification to calculating an equilibrium ice table agnostic to the lithic content of the ice.

1.2.3   Incidence angle and orbit

The elevation β of the sun above an horizontal horizon is given in terms of geographic latitude λ, declination δ of the sun, and the hour angle h by

$$\sin \beta = \cos \lambda \cos \delta \cos h + \sin \lambda \sin \delta. \tag{1.12}$$

Equations for the ephemerides of present-day Mars are implented in `marsorbit.f90`. For past orbital elements, `generalorbit.f` can be used, which solves Kepler's equation with the Newton method.

1.2.4   Mars atmospheric extinction and sky irradiance

The absorbed direct solar irradiance is approximately

$$Q_{\text{solar}} = \frac{S_0}{R^2}(1 - A)(1 - f)^{1/\max(\sin \beta, 0.04)} \sin \beta, \tag{1.13}$$

9

where S_0 is the solar constant, R the distance from the sun in AU, A the albedo, and f due to the extinction in the atmosphere. The length of the path through the atmosphere is approximately proportional to $1/\sin \beta$ and the transmission is taken to be exponential in this path length. The nadir optical depth of the atmosphere is $-\ln(1 - f) \approx f$. For small extinction and away from the horizon, $(1-f)^{1/\sin \beta} \approx 1-f/\sin \beta$. The maximum atmospheric path length ℓ_{max} is limited due to the curvature of the planet, $H/\ell_{\mathrm{max}} \approx \sqrt{H/2R} \approx 0.04$ for Mars, where H is the scale height of the atmosphere and R the radius of the planet.

In addition to the direct insolation, the diffuse irradiance from the sky contributes to the surface energy balance (sky irradiance). Atmospheric emission is approximated by a fraction f_{IR} (typically 2–4%) of noontime insolation and is kept constant throughout a solar day (Kieffer et al., 1977):

$$Q_{\mathrm{a,IR}} = f_{\mathrm{IR}} \frac{S_0}{R^2} \sin \beta_{\mathrm{noon}} \qquad \text{(all day)} \tag{1.14}$$

This approximation fails in the polar regions; in this case, Kieffer et al. (1977) replaces the noontime insolation with the surface frost emission.

In addition, there is scattered light when $\sin \beta > 0$, which is approximated by

$$Q_{\mathrm{a,scat}} = \frac{1}{2} f_{\mathrm{scat}} \frac{S_0}{R^2}. \tag{1.15}$$

Half of the scattered light is assumed to be lost to space.

For the purpose of discussion, we determine the total energy budget of the atmosphere for a horizontal land mass. To first order $(1 - f)^{1/\sin \beta} \sin \beta \approx \sin \beta - f$, in eq. (1.13), so at any time the sun is above the horizon the energy absorbed and scattered in the atmosphere is approximately $(S_0/R^2)f$. Over a solar day

$$\frac{S_0}{R^2} f \int_{\mathrm{daytime}} dh \approx \frac{S_0}{R^2} \pi f. \tag{1.16}$$

The infrared emission from the atmosphere over the same time period is

$$2\pi f_{\mathrm{IR}} \frac{S_0}{R^2} \sin \beta_{\mathrm{noon}} \tag{1.17}$$

and the scattered energy

$$\pi f_{\mathrm{scat}} \frac{S_0}{R^2}. \tag{1.18}$$

The globally averaged $\sin \beta_{\mathrm{noon}}$ is

$$\frac{1}{\pi} \int_{-\pi/2}^{\pi/2} d\lambda \cos \lambda \sin \beta_{\mathrm{noon}} \approx \frac{1}{\pi} \int_{-\pi/2}^{\pi/2} d\lambda \cos^2 \lambda = \frac{1}{2} \tag{1.19}$$

Global balance, (1.16)=(1.17)+(1.18), is achieved with $f = f_{\mathrm{IR}} + f_{\mathrm{scat}}$. This relation does not hold at an individual latitude, but it does hold globally.

1.3 Surface Energy Balance for Planar Slope on Mars

Planar slopes are much simpler than the general 3D problem. This section describes a model for the thermal balance on a tilted plane, in the form of two coupled 1D thermal models, plus a quasi-0D atmosphere. The model is for Mars, but easily simplified to airless bodies. It was used in Aharonson and Schorghofer (2006) and Schorghofer and Edgett (2006).

History: developed 2002–2005

1.3.1 Direct solar irradiance on slope

The elevation β of the sun above a horizontal horizon is given by (1.12). The angle θ of the sun above a sloped surface is

$$\sin\theta = \cos\alpha \sin\beta - \sin\alpha \cos\beta \cos(\Delta a), \tag{1.20}$$

where α is the slope angle and Δa is the difference between the azimuth of the sun and the azimuth of the topographic gradient. The sun is assumed to be below the horizon if either $\sin\beta < 0$ (horizontal horizon at infinity) or $\sin\theta < 0$ (self shadowing of slope).

On an airless body the direct insolation is

$$Q_{\text{solar}} = \frac{S_0}{R^2}(1-A)\sin\theta. \tag{1.21}$$

where S_0 is the solar constant, R the distance from the sun in AU, and A the albedo.

For Mars, the direct solar insolation is

$$Q_{\text{solar}} = \frac{S_0}{R^2}(1-A)(1-f)^{1/\max(\sin\beta, 0.04)}\sin\theta, \tag{1.22}$$

where f arises from the extinction in the atmosphere. This is a generalization of eq. (1.13) in subsection 1.2.4, where this approximate expression is further justified.

1.3.2 Approximate terrain and sky irradiance for planar slope

Let α denote the slope angle. The heat balance on the surface is given by (1.11), with

$$Q = Q_{\text{solar}}(\alpha) + Q_{\text{a,IR}}(\alpha) + Q_{\text{a,scat}}(\alpha) + Q_{\text{land}}(\alpha). \tag{1.23}$$

Q is the absorbed irradiance from the sun, atmosphere, and surfaces within field of view. The subscript a denotes contributions from the atmosphere. Figure 1.4 illustrates the contributions.

Terrain irradiance: The surface reemits radiation in all directions, but receives additional energy from surfaces in its field of view (terrain irradiance). This emission is weighted according to the incidence angle ι (Greek letter iota) and integrated over the spherical angle Ω subtended by the visible land surfaces. If we consider a horizontal surface at uniform temperature T_2 (Kreslavsky and Head, 2005):

$$Q_{\text{land}} = \epsilon_2 \sigma T_2^4 \int \cos\iota \, d\Omega = \sin^2\left(\frac{\alpha}{2}\right)\epsilon_2 \sigma T_2^4. \tag{1.24}$$
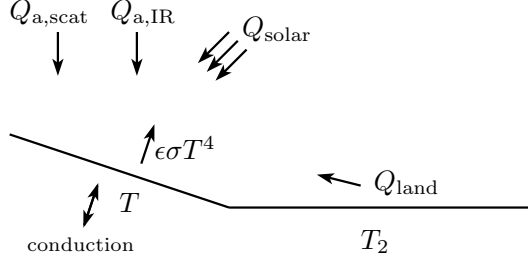
Figure 1.4: Contributions to the heat balance on a slope with surface temperature T.

If one assumes $T_2 = T$ and $\epsilon_2 = \epsilon$, then this term can be brought to the right-hand side of eq. (1.11), leading to an effective emissivity of $\epsilon \cos^2(\alpha/2)$. However, this is often not a good approximation, as demonstrated in Aharonson and Schorghofer (2006), Fig. 2b. It is more accurate to base T_2 on a separate 1D model for a flat surface.

Sky irradiance for planar slope. The diffuse irradiance from the sky adds a small amount of energy to the surface. In the spirit of the Kieffer approximation (subsection 1.2.4),

$$Q_{\text{a,IR}} = \frac{S_0}{R^2} F_{\text{sky}} f_{\text{IR}} \sin \beta_{\text{noon}} \qquad \text{(all day)} \qquad (1.25)$$

and if the sun is up, then

$$Q_{\text{a,scat}} = \frac{S_0}{2R^2}(1 - A) F_{\text{sky}} f_{\text{scat}} \qquad \text{when } \sin \beta > 0 \qquad (1.26)$$

otherwise $Q_{\text{a,scat}} = 0$.

More than one definition of (sky) view factor F_{sky} and various approximations for the sky irradiance are used in the literature; see Flo Heggem et al. (2001) and Rakovec and Zakšek (2012). For isotropic (Lambertian) irradiance from the sky, the diffuse irradiance from the atmosphere is weighed by the cosine of the incidence angle. For a planar slope this results in $F_{\text{sky}} = \cos^2(\alpha/2)$.

Spiga and Forget (2008) have derived a more detailed parameterization for $Q_{\text{a,scat}}$ on a planar slope on Mars.

Bibliography

Aharonson, O. and Schorghofer, N., 2006. Subsurface ice on Mars with rough topography. *J. Geophys. Res.* 111(E11):E11007. doi: 10.1029/2005JE002636.

Crank, J. and Nicolson, P., 1947. A practical method for numerical evaluation of solutions of partial differential equations of the heat-conduction type. *Mathematical Proceedings of the Cambridge Philosophical Society* 43(1):50–67.

Flo Heggem, E. S., Etzelmüller, B., and Berthling, I., 2001. Topographic radiation balance models: sensitivity and application in periglacial geomorphology. *Norsk Geografisk Tidsskrift-Norwegian Journal of Geography* 55(4):203–211. doi: 10.1080/00291950152746531.

Handelsman, R. A. and Olmstead, W. E., 1972. Asymptotic solution to a class of nonlinear Volterra integral equations. *SIAM J. Appl. Math.* 22(3):373–384. doi: 10.1137/0122035.

Kieffer, H. H., Martin, T. Z., Peterfreund, A. R., Jakosky, B. M., Miner, E. D., and Palluconi, F. D., 1977. Thermal and albedo mapping of Mars during the Viking primary mission. *J. Geophys. Res.* 82(28):4249–4291. doi: 10.1029/JS082i028p04249.

Kreslavsky, M. A. and Head, J. W., 2005. Mars at very low obliquity: atmospheric collapse and the fate of volatiles. *Geophys. Res. Lett.* 32(12):L12202. doi: 10.1029/2005GL022645.

Lide, D. R., editor, 2003. *CRC Handbook of Chemistry and Physics.* CRC Press, 84th edition.

Press, W. H., Teukolsky, S. A., Vetterling, W. T., and Flannery, B. P., 1992. *Numerical Recipes in C.* Cambridge University Press, New York, second edition.

Rakovec, J. and Zakšek, K., 2012. On the proper analytical expression for the sky-view factor and the diffuse irradiation of a slope for an isotropic sky. *Renewable Energy* 37(1): 440–444. doi: 10.1016/j.renene.2011.06.042.

Schorghofer, N., 2008. Temperature response of Mars to Milankovitch cycles. *Geophys. Res. Lett.* 35:L18201. doi: 10.1029/2008GL034954.

Schorghofer, N. and Aharonson, O., 2005. Stability and exchange of subsurface ice on Mars. *J. Geophys. Res.* 110(E5):E05003. doi: 10.1029/2004JE002350.

Schorghofer, N. and Edgett, K. S., 2006. Seasonal surface frost at low latitudes on Mars. *Icarus* 180(2):321–334. doi: 10.1016/j.icarus.2005.08.022.

Siegler, M., Aharonson, O., Carey, E., Choukroun, M., Hudson, T., Schorghofer, N., and Xu, S., 2012. Measurements of thermal properties of icy Mars regolith analogs. *J. Geophys. Res.* 117:E03001. doi: 10.1029/2011JE003938.

Spiga, A. and Forget, F., 2008. Fast and accurate estimation of solar irradiance on martian slopes. *Geophys. Res. Lett.* 35:L15201. doi: 10.1029/2008GL034956.

Winter, D. F. and Saari, J. M., 1969. A particulate thermophysical model of the lunar soil. *Astrophys. J.* 156:1135–1151.

Part 2

Diffusion of Water Vapor with Phase Transitions

1-Dimensional Diffusion of Water Vapor in Porous Medium with Phase Transitions;
variable diffusivity; irregular grid
3 phases: vapor, free (macroscopic) H_2O ice, H_2O adsorbate
implemented in `vapordiffusioni.f`

History: developed 2003–2004

2.1 Governing Equations

indices: v ... gas (vapor), f ... free ice (solid), a ... adsorbed water
$\bar{\rho}$ ... mass per total volume, $\bar{J}$ ... vapor flux per total area

conservation of mass:
$$\frac{\partial}{\partial t}(\bar{\rho}_v + \bar{\rho}_f + \bar{\rho}_a) + \nabla \cdot \bar{J} = 0 \tag{2.1}$$

vapor transport: (Landau and Lifshitz, 1987, Vol. VI, §57, §58)

$$J = -D\rho_0 \nabla c \tag{2.2}$$

c ... concentration $c = \rho_v/\rho_0$
ρ_0 ... total density of air, including water vapor
ρ_v ... density of vapor

$$p_v = nkT = \rho_v \frac{k}{m_v} T \tag{2.3}$$

m_v ... mass of water molecule; k ... Boltzmann constant

ϵ ... porosity (= void space / total volume)
$\epsilon(1 - \rho_f/\rho_{\text{ice}})$ ... fraction of space available to gas
$\bar{\rho}_v = \rho_v \epsilon (1 - \rho_f/\rho_{\text{ice}})$ ρ_v ... vapor density in void space
$\bar{\rho}_f = \rho_f \epsilon$ ρ_f ... ice density in volume not occupied by regolith
$\bar{J} = J\epsilon(1 - \rho_f/\rho_{\text{ice}})$ J ... vapor flux through void area
$\rho_{\text{ice}} \approx 926 \text{ kg/m}^3$ ... density of ice when it's really cold

adsorption: $\bar{\rho}_a = A(p, T)$ reversible and not kinetically-limited

Conservation of mass becomes

$$\frac{\partial}{\partial t}\left(\rho_v\left(1 - \frac{\rho_f}{\rho_{\text{ice}}}\right) + \rho_f + \frac{1}{\epsilon}\bar{\rho}_a\right) + \partial_z\left(1 - \frac{\rho_f}{\rho_{\text{ice}}}\right)J = 0$$

$$\frac{\partial}{\partial t}\left[\rho_v\left(1 - \frac{\rho_f}{\rho_{\text{ice}}}\right) + \rho_f + \frac{1}{\epsilon}\bar{\rho}_a\right] = \partial_z\left[\left(1 - \frac{\rho_f}{\rho_{\text{ice}}}\right)D\partial_z\rho_v\right]$$

introduce $\varphi = 1 - \dfrac{\rho_f}{\rho_{\text{ice}}}$ and $\gamma = \dfrac{k}{m}\dfrac{1}{\epsilon}$

$$\partial_t\left(\frac{p}{T}\varphi + \frac{k}{m_v}\rho_f\right) + \gamma\left(\frac{\partial\bar{\rho}_a}{\partial p}\partial_t p + \frac{\partial\bar{\rho}_a}{\partial T}\partial_t T\right) = \partial_z\left[D\varphi\left(\partial_z\frac{p}{T}\right)\right] \tag{2.4}$$

This is an equation for p and ρ_f.

If there is no ice, then

$$\left(\frac{1}{T} + \gamma\frac{\partial\bar{\rho}_a}{\partial p}\right)\partial_t p + \left(-\frac{p}{T^2} + \gamma\frac{\partial\bar{\rho}_a}{\partial T}\right)\partial_t T = \partial_z\left(D\partial_z\frac{p}{T}\right)$$

2.2 Discretizations

2.2.1 Possible discretizations of spatial derivatives

Note: These spatial discretizations are not necessarily optimal in terms of discretization error.

$$\partial_z(a\partial_z b)|_j = \frac{1}{\Delta z^2}\left(a_{j+1/2}(b_{j+1} - b_j) - a_{j-1/2}(b_j - b_{j-1})\right) + O(\Delta z^2) \tag{2.5}$$

or

$$\partial_z(a\partial_z b)|_j = \frac{1}{2\Delta z^2}\left((a_{j+1} + a_j)(b_{j+1} - b_j) - (a_j + a_{j-1})(b_j - b_{j-1})\right) + O(\Delta z^2) \tag{2.6}$$

or

$$\partial_z(a\partial_z b)|_j = a\partial_{zz}b + (\partial_z a)\partial_z b$$

$$= \frac{1}{\Delta z^2}\left[a_j(b_{j+1} - 2b_j + b_{j-1}) + \frac{1}{4}(a_{j+1} - a_{j-1})(b_{j+1} - b_{j-1})\right] + O(\Delta z^2) \tag{2.7}$$

The most general discretization which is accurate to $O(\Delta z^2)$, rather than just $O(\Delta z)$, is of the following form (mathematica notebook discretization2.nb)

$$
\begin{aligned}
\partial_z(a\partial_z b)|_j = \quad & \frac{1}{\Delta z^2}(ca_j b_j + (-1 - \frac{c}{2})a_{j-1}b_j + (-1 - \frac{c}{2})a_{j+1}b_j \\
& -\frac{c}{2}a_j b_{j-1} + \frac{3+c}{4}a_{j-1}b_{j-1} + \frac{1+c}{4}a_{j+1}b_{j-1} \\
& -\frac{c}{2}a_j b_{j+1} + \frac{1+c}{4}a_{j-1}b_{j+1} + \frac{3+c}{4}a_{j+1}b_{j+1}) + O(\Delta z^2) \tag{2.8}
\end{aligned}
$$

15

Choices (2.6) and (2.7) above correspond to $c = -1$ and $c = -2$, respectively.

Another set of schemes does not involve the cross-terms $a_{j+1}b_{j-1}$ and $a_{j-1}b_{j+1}$. They are of the following form (mathematica notebook discretization3.nb)

$$
\begin{aligned}
\partial_z(a\partial_z b)|_j &= \frac{1}{\Delta z^2}(-a_j b_j - c a_{j-1} b_j + (-1+c)a_{j+1} b_j + \\
&\quad (1-c)a_j b_{j-1} + c a_{j-1} b_{j-1} + c a_j b_{j+1} + (1-c)a_{j+1} b_{j+1}) + \\
&\quad \left(c - \frac{1}{2}\right) O(\Delta z) + O(\Delta z^2) \\
&= \frac{1}{\Delta z^2}[(1-c)a_{j+1}(b_{j+1} - b_j) + c a_{j-1}(b_{j-1} - b_j) + \\
&\quad + a_j(c b_{j+1} - b_j + (1-c)b_{j-1})] + O(\Delta z)
\end{aligned}
\tag{2.9}
$$

For $c = 1/2$ this reduces to scheme (2.6) above
If starting with complete pore filling, $c > 0$ is required for downward motion of ice table.

On irregular grid: General scheme without cross-terms (mathematica notebook discretization6.nb)

$$
\begin{aligned}
\partial_z(a\partial_z b)|_j &= -\frac{2c + (1-2c)h_+/h_-}{h_- h_+} a_j b_j + \frac{-1 + (1-2c)h_+/h_-}{h_-(h_- + h_+)} a_{j-1} b_j + \frac{2c - 2}{h_+(h_- + h_+)} a_{j+1} b_j + \\
&\quad + \frac{1 + (1-2c)h_+/h_-}{h_-(h_- + h_+)} a_j b_{j-1} + \frac{1 + (2c-1)h_+/h_-}{h_-(h_- + h_+)} a_{j-1} b_{j-1} + \frac{2c}{h_+(h_- + h_+)} a_j b_{j+1} \\
&\quad + \frac{2 - 2c}{h_+(h_- + h_+)} a_{j+1} b_{j+1} + O(h_+ + h_-)
\end{aligned}
\tag{2.10}
$$

where $h_+ = z_{j+1} - z_j$ and $h_- = z_j - z_{j-1}$. For $h_+ = h_- = h$ this reduces to (2.9)

2.2.2 Discretization of time derivative

use eq. (2.4), $A \equiv f$

$$
\begin{aligned}
\frac{p_j^{n+1}}{T_j^{n+1}}\varphi_j^{n+1} - \frac{p_j^n}{T_j^n}\varphi_j^n + \frac{k}{\mu}\left(\rho_{f_j}^{n+1} - \rho_{f_j}^n\right) + \gamma \left.\frac{\partial f}{\partial p}\right|_j^n (p_j^{n+1} - p_j^n) + \\
+\gamma \left.\frac{\partial f}{\partial T}\right|_j^n (T_j^{n+1} - T_j^n) = \Delta t \left(\partial_z D \varphi \partial_z \frac{p}{T}\right)_j^n
\end{aligned}
\tag{2.11}
$$

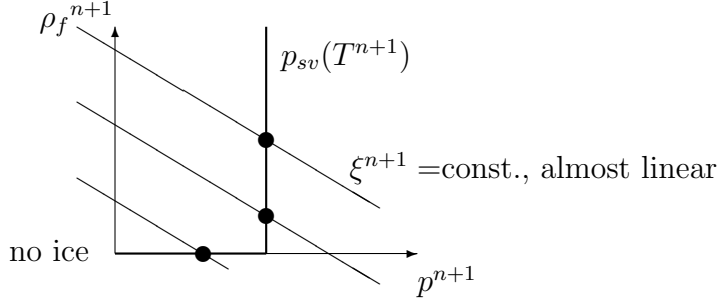derivatives of the isotherm are not expanded to keep it linear

2.2.3 Complete scheme

using (2.11) and (2.10)

$$
\xi_j^{n+1} = \frac{p_j^n}{T_j^n}\varphi_j^n + \frac{k}{\mu}\rho_{f_j}^n + \gamma \left.\frac{\partial f}{\partial p}\right|_j^n p_j^n - \gamma \left.\frac{\partial f}{\partial T}\right|_j^n (T_j^{n+1} - T_j^n) +
$$

$$\frac{\Delta t}{\Delta z^2} \left[D_j \varphi_j^n \left(\frac{p_{j+1}^n}{T_{j+1}^n} - 2\frac{p_j^n}{T_j^n} + \frac{p_{j-1}^n}{T_{j-1}^n} \right) + \frac{1}{4}(D_{j+1}\varphi_{j+1}^n - D_{j-1}\varphi_{j-1}^n) \left(\frac{p_{j+1}^n}{T_{j+1}^n} - \frac{p_{j-1}^n}{T_{j-1}^n} \right) \right]$$

where $\xi^{n+1} = \dfrac{p^{n+1}}{T^{n+1}} \left(1 - \dfrac{\rho_f^{n+1}}{\rho_{\text{ice}}} \right) + \dfrac{k}{\mu}\rho_f^{n+1} + \gamma \left. \dfrac{\partial f}{\partial p} \right|^n p^{n+1}$

$p \le p_{sv}(T)$ and $0 \le \rho_f \le \rho_{\text{ice}}$

p_{sv} ... saturation vapor pressure

Try $\rho_f^{n+1} = 0 \quad \Rightarrow \quad p^{n+1} = \dfrac{T^{n+1} \cdot \xi^{n+1}}{1 + T^{n+1}\gamma \left. \frac{\partial f}{\partial p} \right|^n} \quad$ and $\quad \rho_f^{n+1} = 0$

If $\quad p^{n+1} > p_{sv}(T^{n+1}) \quad$ then $\quad p^{n+1} = p_{sv}(T^{n+1}) \quad$ and

$$\rho_f^{n+1} = \frac{\xi^{n+1} - \frac{p_{sv}(T^{n+1})}{T^{n+1}} - \gamma \left. \frac{\partial f}{\partial p} \right|^n p_{sv}(T^{n+1})}{\frac{k}{\mu} - \frac{p_{sv}(T^{n+1})}{T^{n+1}\rho_{\text{ice}}}}$$

introduce $\quad p_{\text{frost}}^{n+1} = p_{sv}(T^{n+1})$

2.2.4 Upper boundary condition

1) $p(z = 0, t) = p_{\text{atm.}}(t)$
2) $D(z = 0) = D_0$
3) $\varphi_0 = 1$

$$\left. \partial_z \left(D\varphi \partial_z \frac{p}{T} \right) \right|_{j=0} = \frac{1}{\Delta z^2} \left[D_1\varphi_1 \left(\frac{p_2}{T_2} - 2\frac{p_1}{T_1} + \frac{p_{\text{atm}}}{T_{\text{surf}}} \right) + \frac{1}{4}(D_2\varphi_2 - D_0\varphi_0) \left(\frac{p_2}{T_2} - \frac{p_{\text{atm}}}{T_{\text{surf}}} \right) \right]$$
$$(2.12)$$

for half-shifted grid ($z_2 = 3z_1$):

$$a\partial_{zz}b + (\partial_z a)\partial_z b = \frac{1}{\Delta z^2} \left[a_1 \left(\frac{8}{3}b_s - 4b_1 + \frac{4}{3}b_2 \right) + \left(-\frac{4}{3}a_s + a_1 + \frac{1}{3}a_2 \right) \left(-\frac{4}{3}b_s + b_1 + \frac{1}{3}b_2 \right) \right]$$
$$(2.13)$$

2.2.5 Lower boundary condition

no vapor flux (impermeable) $J = 0 \quad \Rightarrow \quad \partial_z \rho_v = 0 \quad \Rightarrow \quad \partial_z \frac{p}{T} = 0 \quad \Rightarrow \quad \frac{p_{N+1}}{T_{N+1}} = \frac{p_{N-1}}{T_{N-1}}$

$$\partial_z \left(D\varphi \partial_z \frac{p}{T} \right)\Big|_{j=N} = \frac{1}{\Delta z^2} 2 D_N \varphi_N \left(\frac{p_{N-1}}{T_{N-1}} - \frac{p_N}{T_N} \right) \tag{2.14}$$

2.3 Discussion

For 1D diffusion and advection with multiple gases, the governing equations are more complex, but the numerical implementation is not. For the governing equations in non-isothermal environments see works such as Cunningham and Williams (1980); Bouziani and Fanale (1998); Hudson et al. (2007).

Water vapor diffusion calculations for Mars are carried out in Schorghofer and Aharonson (2005).

Bibliography

Bouziani, N. and Fanale, F. P., 1998. Physical chemistry of a heterogeneous medium: Transport processes in comet nuclei. *Astrophys. J.* 499(1):463. doi: 10.1086/305599.

Cunningham, R. and Williams, R., 1980. *Diffusion in Gases and Porous Media.* Plenum Press, New York.

Hudson, T. L., Aharonson, O., Schorghofer, N., Farmer, C. B., Hecht, M. H., and Bridges, N. T., 2007. Water vapor diffusion in Mars subsurface environments. *J. Geophys. Res.* 112(E5):E05016. doi: 10.1029/2006JE002815.

Landau, L. D. and Lifshitz, E. M., 1987. *Fluid Mechanics.* Pergamon Press, Oxford.

Schorghofer, N. and Aharonson, O., 2005. Stability and exchange of subsurface ice on Mars. *J. Geophys. Res.* 110(E5):E05003. doi: 10.1029/2004JE002350.

Part 3

Long-Term Ice Evolution: Equilibrium and Non-equilibrium Ice Tables

Long-term evolution of sub-surface ice due to vapor exchange with the atmosphere using diurnally- and seasonally-resolved temperatures.

History:
    2002–2004 equilibrium ice table on Mars
    2006–2011 asynchronous model for ice on Mars

3.1 Equilibrium Ice Table on Mars

The equilibrium depth to the ice table is defined by a balance between the vapor pressure at the ice table and the atmosphere (Fig. 3.1). It is the end result of atmosphere-subsurface vapor exchange after an asymptotically long time. If no equilibrium is possible, then subsurface ice is "unstable". Using the thermal model described in Part 1, this model calculates the equilibrium depth based on matching the vapor density at the ice table with that in the atmosphere. The thermal model is run over a number of Mars years to equilibrate, and annual means are calculated for the last orbit. The ice content of the subsurface changes the thermal properties, and the thermal model is repeatedly equilibrated.

    Figure 3.2 shows the result of thermal model calculations (using the methods described
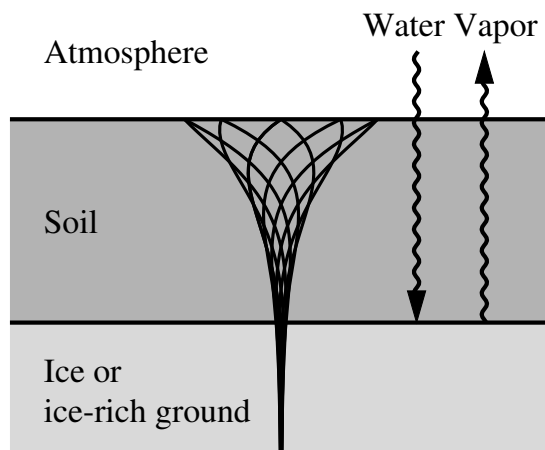

Figure 3.1: Subsurface ice exchanges water vapor with the atmosphere through a layer of porous soil. Temperature oscillations decay with depth, as illustrated by a set of instantaneous temperature profiles.

in Part 1) and vapor diffusion calculations (using the methods described in Part 2). The gradient in temperature changes at the ice table due to the change in thermal properties (Fig. 3.2a). The annual mean of the vapor density profile can be determined from the annual mean of the vapor density on the surface and at the ice table (Fig. 3.2c). The time-averaging can be justified mathematically by swapping the time integral with the gradient in Fick's diffusion law. These boundary values can be calculated without solving the vapor diffusion equation, which provides a major computational advantage.
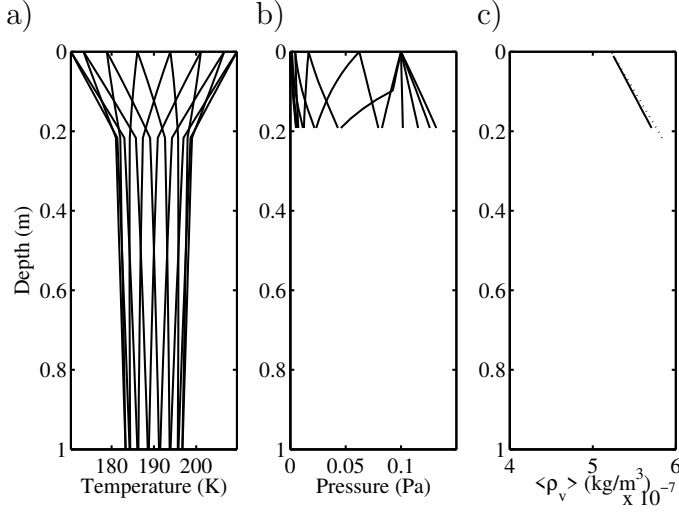

Figure 3.2: Temperature, partial pressure of H_2O, and annual mean vapor density $\langle \rho_v \rangle$ when the ice table is above equilibrium (and therefore retreats). In this conceptual example, a sinusoidal surface temperature dependence is assumed. The vapor density profiles vary with time, but the annual mean of ρ_v simply increases linearly with depth. The dotted line is based on the boundary values of the mean annual vapor density and closely approximates the annual mean from the microphysical vapor diffusion calculations.

The equilibrium ice table calculations determine at what depth the annual mean vapor density at the ice table matches that on the surface. Because the ice content changes the thermal properties, multiple thermal model runs need to be carried out to arrive at the equilibrium depth. A root-finding procedure is deployed to find the equilibrium depth. In `mars_mapi.f` the root-finding procedure is a bisection method. The more recent but simpler program `mars_mapii.f` instead iteratively updates the instantaneous equilibrium depth to arrive at the unique final equilibrium depth. Then `mars_mapt.f` can be used to output additional variables for a given ice table depth.

The model was extensively used in Schorghofer and Aharonson (2005), where further description is available. With extensions described in section 1.3.2 for planar slopes, it also forms the core of the model used in Aharonson and Schorghofer (2006).

3.2   Asynchronous Model for Near-Surface Ice on Mars

The model couples a diurnally-resolved thermal model with a long-term ice evolution model. Ice (massive or interstitial) can be lost to the atmosphere and, vice-versa, pore spaces can

Table 3.1: Programs that calculate the equilibrium ice table on Mars.

Main program	Task
mars_mapt	temperatures for prescribed ice table depth
mars_mapi	finds equilibrium ice table with bisection method
mars_mapii	finds equilibrium ice table with iteration method
mars_mapi2p	finds equilibrium ice table for planar slopes with bisection method

be recharged with interstitial ice. In difference to the model for the equilibrium ice table (section 3.1), this *dynamical* model calculates changes in ice volume and the interstitial spaces may only be partially filled with ice.

Schorghofer (2010) provides a description of this rather complex model, which is not repeated here. In brief, the time-averaged vapor transport equations are solved, which avoids having to solve the microphysical vapor transport equations. The numerical method involves a one-sided derivative at the moving ice table, otherwise a numerical instability occurs due to the strong contrast in thermal properties at the ice table. The model allows for up to three layers: ice-free, soil with interstitial ice (plus void spaces), and massive ice with dust. In the current implementation, one of the two interfaces is tracked explicitly. The model is extensively used in Schorghofer (2007) and Schorghofer and Forget (2012) for studies of the Martian Ice Age cycle.

Table 3.2: Overview of current implementations of asynchronous dynamic models for Mars

Main program	Task
mars_fast	ice evolution on Mars (massive and interstitial ice)
exper_fast	ice evolution in lab experiment
stabgrow_fast	growth of pore ice

Bibliography

Aharonson, O. and Schorghofer, N., 2006. Subsurface ice on Mars with rough topography. *J. Geophys. Res.* 111(E11):E11007. doi: 10.1029/2005JE002636.

Schorghofer, N., 2007. Dynamics of ice ages on Mars. *Nature* 449(7159):192–194. doi: 10.1038/nature06082.

Schorghofer, N., 2010. Fast numerical method for growth and retreat of subsurface ice on Mars. *Icarus* 208(2):598–607. doi: 10.1016/j.icarus.2010.03.022.

Schorghofer, N. and Aharonson, O., 2005. Stability and exchange of subsurface ice on Mars. *J. Geophys. Res.* 110(E5):E05003. doi: 10.1029/2004JE002350.

Schorghofer, N. and Forget, F., 2012. History and anatomy of subsurface ice on Mars. *Icarus* 220(2):1112–1120. doi: 10.1016/j.icarus.2012.07.003.